

Major Technical Advances from the Work of Staehle and Collaborators

Corrosion Engineering

- Developed the “corrosion based design approach” (CBDA) for predicting and assuring performance and for analyzing failures.
- Developed the “location for analysis matrix” (LAM) for organizing the information necessary to predict and assure performance and for analyzing failures.
- First to demonstrate, as in Figure 1, that the occurrence of stress corrosion cracking in nuclear steam generators could be modeled with Weibull statistics. (with J. Gorman)

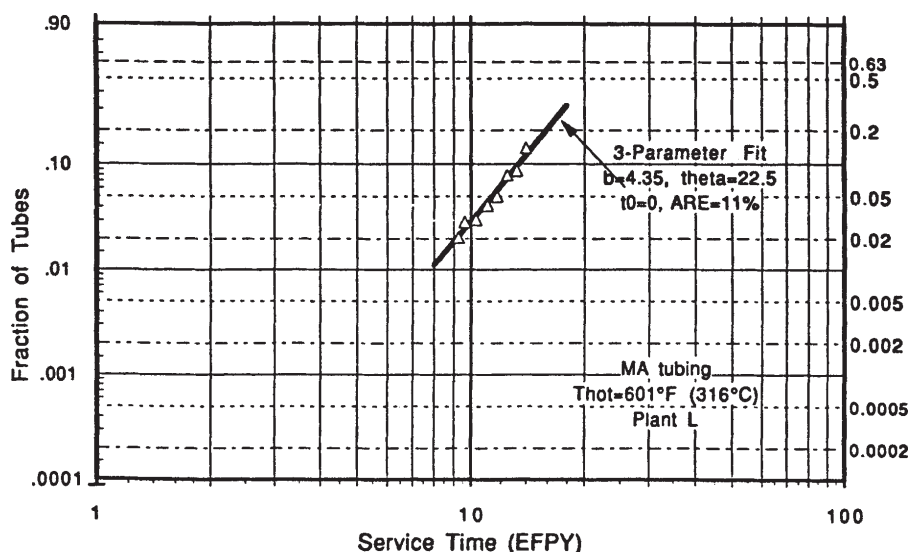


Figure 1 Fraction of tubes failed versus time in Weibull coordinates for intergranular stress corrosion cracking and intergranular corrosion in tubes of nuclear steam generator at tube sheet crevices for a single steam generator.

- First to demonstrate how physical variables could be used to model statistical parameters. (with J. Gorman)
- First to demonstrate that “blue water” observed in homes was produced by microbial action on copper tubes. (with B. Little)
- First recognized and advocated the correlation of plant and laboratory data in nuclear reactor systems using electrochemical methods.
- First demonstrated that the main cause of corrosion and stress corrosion cracking, as in Figure 2, of post tension tendons, except where abundant road salt is present, is the acidic metabolic products of fungi reacting with grease. (with B. Little)

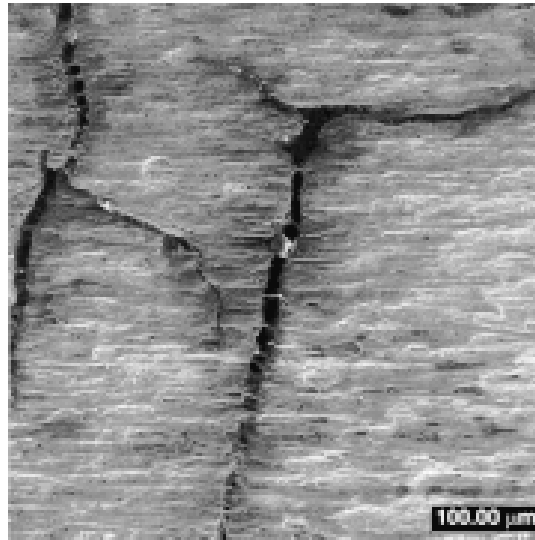


Figure 2 Stress corrosion cracking of drawn steel wire in tendon used in post tension construction due to the action of acids produced by the reaction of fungi with grease.

- Developed first stable pressure balanced reference electrode for work in high temperature water. (with A. Agrawal)
- First to measure the kinetics of electrode reactions in high temperature water. (with G. Welch)
- First to measure the effect of hydrazine on the electrochemical potential in high temperature water. (with A. Agrawal)
- First to measure the behavior of crevices in simulated in vivo applications. (with D. Levine)

Corrosion Science

- First quantitative and physical model, as in Figures 3 and 4, for film rupture mechanism of stress corrosion cracking. (with T. Smith, J. Davis, and T. Murata)

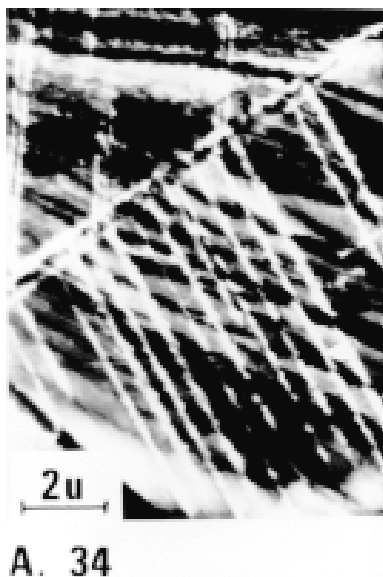


Figure 3 View of dissolution occurring preferentially at slip on metal surface as shown in a thin foil of a Fe-Cr-Ni alloy stressed while exposed to an environment and then viewed in a transmission electron microscope.

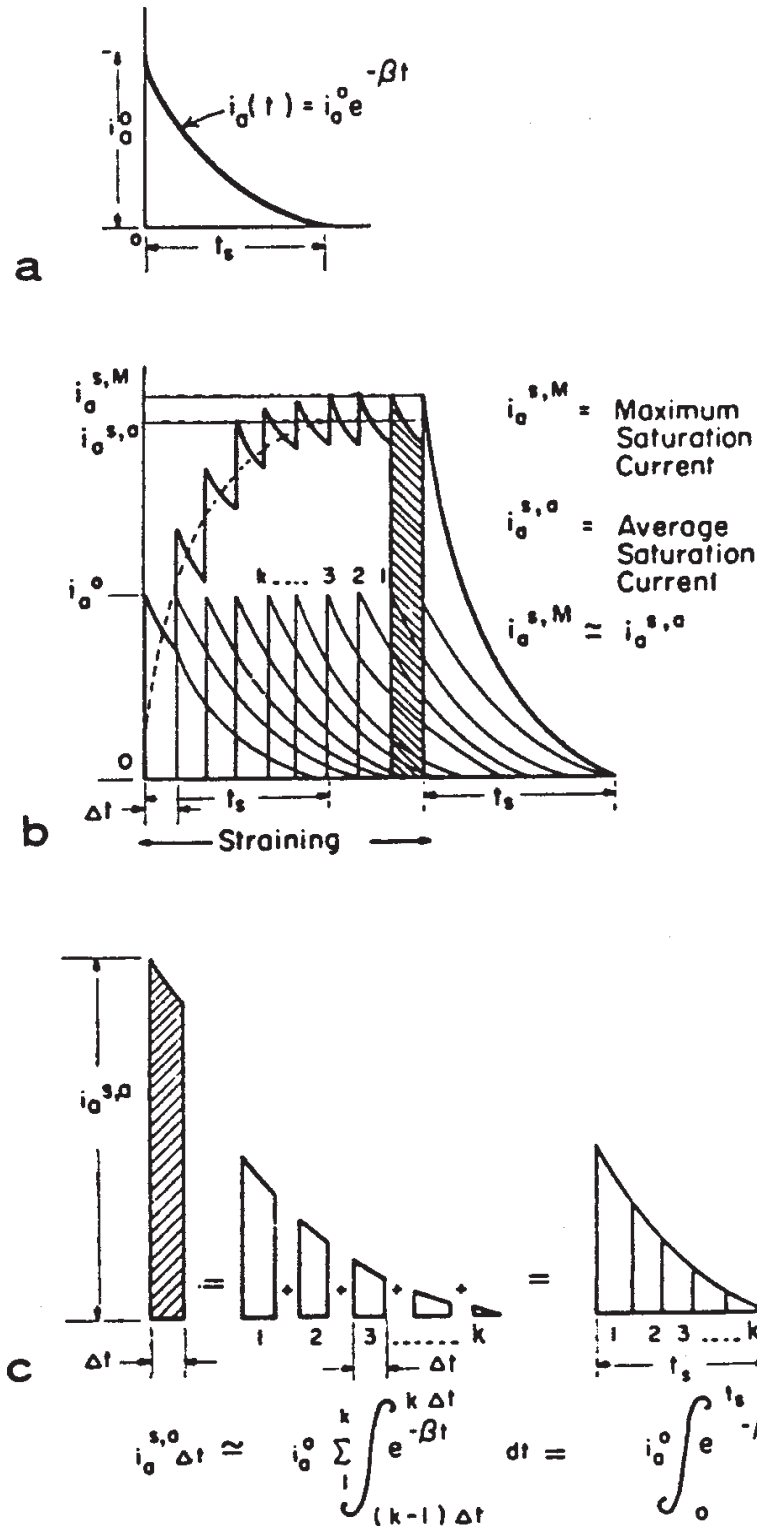


Figure 4 Schematic view of sequential dissolution events as they contribute to an average current for advance of SCC.

- First demonstrated, as in Figure 5, that Cl₂, HBr, HCl and H₂S gases would propagate SCC in high strength steels and that the velocities greatly exceed that for hydrogen alone. (with G. Kerns)

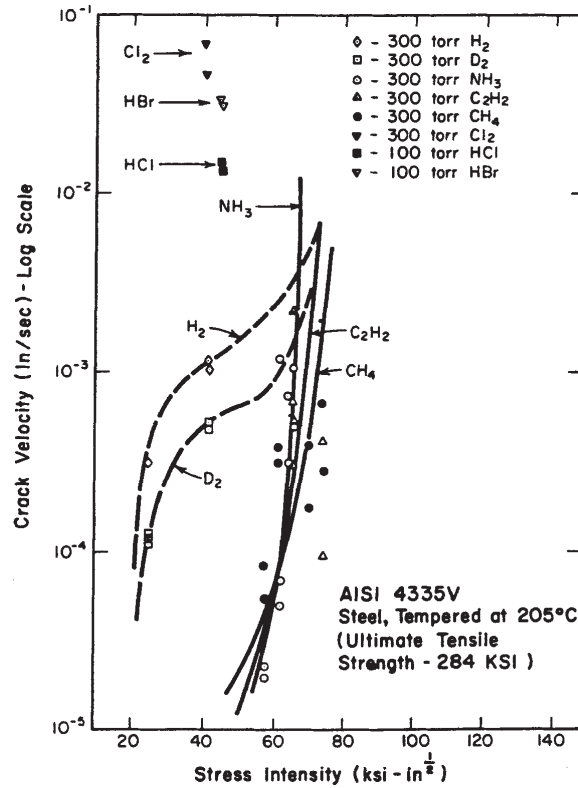


Figure 5 Effect of stress intensity on crack velocity for a high strength steel in gaseous environments.

- First recognized that modes of corrosion such as stress corrosion cracking occurred in regular and predictable patterns in potential-pH space as shown in Figure 6. (with C. Morin)

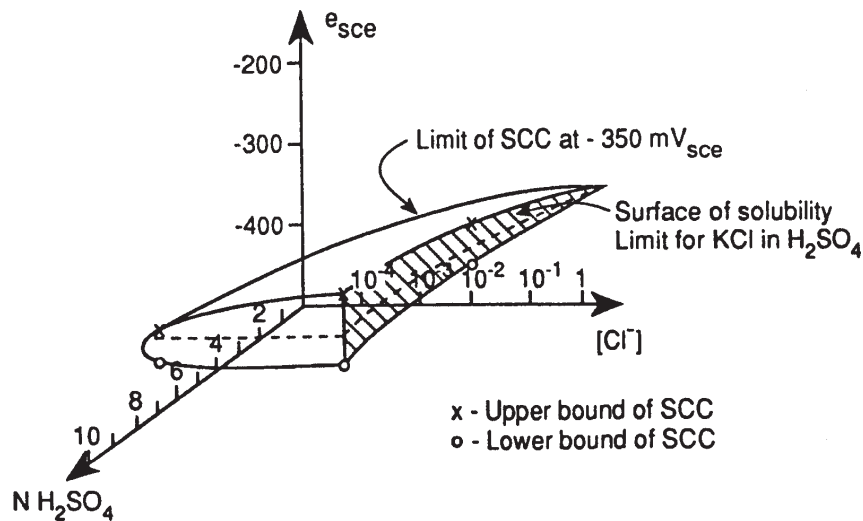


Figure 6 Combined effects of potential, chloride, and sulfuric acid on the occurrence of stress corrosion cracking at room temperature for Type 304L stainless steel.

- First application of Auger analysis to the study of passive films. (with J. B. Lumsden)
- First combined analysis of Auger analysis, ellipsometric and electrochemical methods to the study of passive films (with J. B. Lumsden, M. Seo and S. Smialowska)
- First demonstrated that nickel enriches on the surface of stainless steels exposed to acidic solutions. (with M. Rockel)
- First demonstrated that stress corrosion cracking of pure copper and copper alloys would occur in a broad range of oxidizing conditions as for admiralty brass in sulfate solutions in Figure 7. (with S. Pednekar, A. Agrawal, S. Smialowska)

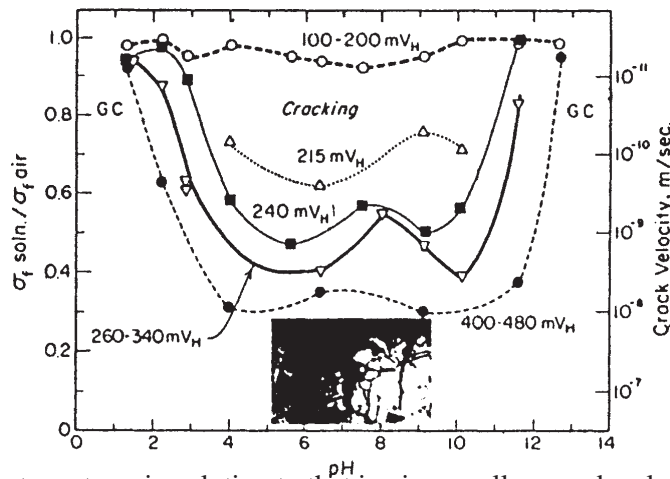


Figure 7 Ratio of fracture stress in solution to that in air as well as crack velocity for admiralty brass in sodium sulfate solution versus pH for different applied potentials. No ammonia present.

- First demonstrated that the structure of high strength steels for the same strength produces significant differences in stress corrosion cracking as in Figure 8. (with M. Wang)

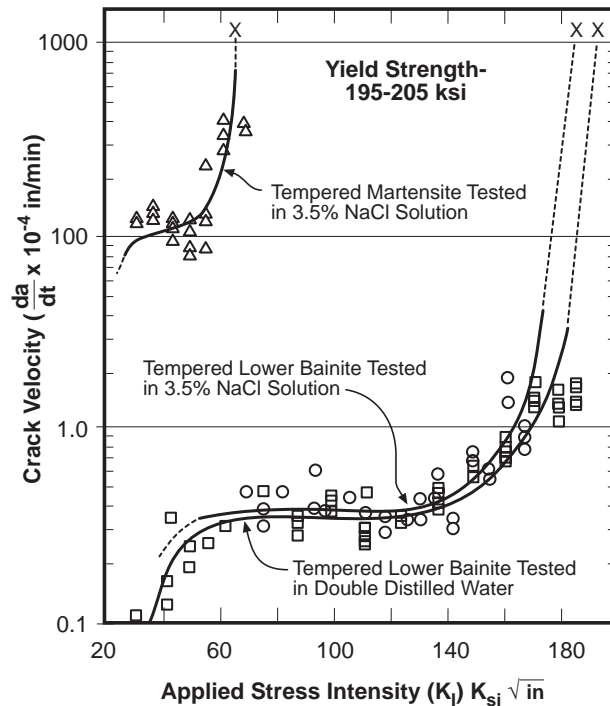


Figure 8 Crack velocity versus stress intensity for a 4340 steel heat treated to produce different structures but with same strength and exposed to room temperature aqueous solutions.

- First developed potential-pH diagram for nickel in high temperature water. (with R. Cowan)
- First demonstrated that slip of single crystals exposed to aqueous solutions is dominated by electrochemical definition. (with R. Latanision)
- First determined the mechanistic action of phosphates, tungstates, and chromates on the passivity of iron. Figure 9 shows the growth in thickness of a phosphate layer. (with S. Smialowska)

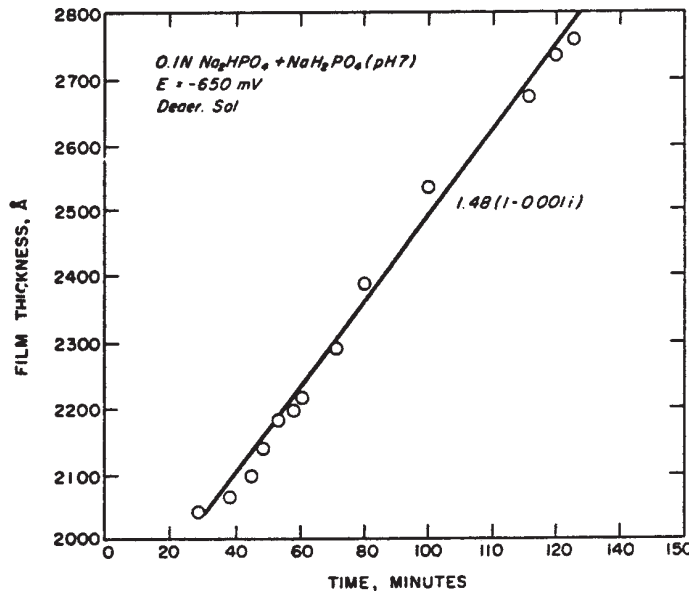


Figure 9 Growth in thickness of a phosphate layer on iron at a deaerated pH of 7 at room temperature and at constant potential. The layer is characterized by a specific complex index.

- First demonstrated that the dissolution of carbides in aqueous solutions would produce either CO₂ or CH₄ reaction products depending on the electrochemical potential as predicted by aqueous thermodynamics. (with J. Payer)
- First interpretation of the combined mechanical and chemical contributions to the activation energy for stress corrosion cracking as shown in Figure 10. (with X-C. Jiang)

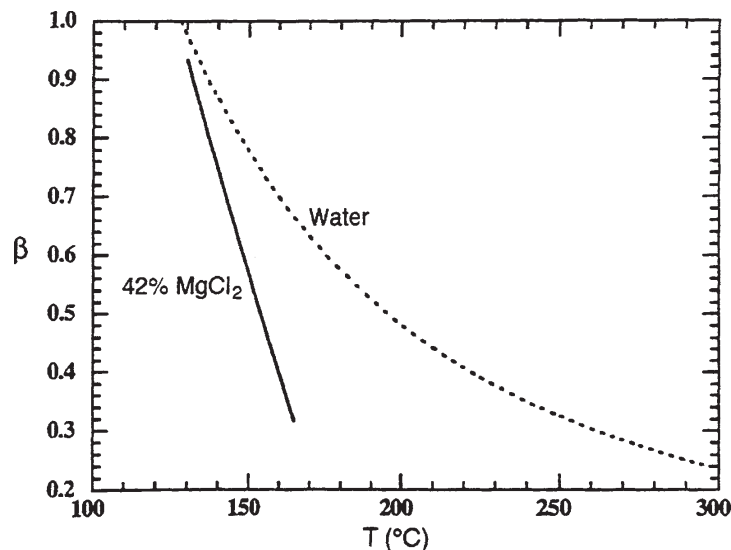


Figure 10 Plot of beta versus temperature for pure water and boiling 42% MgCl₂. Beta is the parameter that indicates what fraction of the activation energy is due to mechanical versus chemical factors.

- First demonstrated that the occurrence of alloying elements in passive films formed in aqueous solutions follows combined predictions based on potential-pH diagrams for individual species. (with J. Lumsden)
- First analysis of the effect of sulfur valence on the steady state and transient passivity of high nickel alloys. Steady state passivity shown in Figure 11. (with Z. Fang)

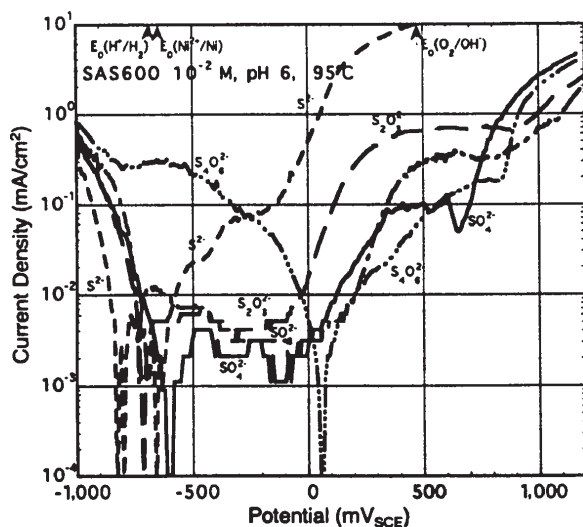


Figure 11 Current density versus applied potential for Alloy 600 exposed to sulfur in aqueous solutions in valences from -2 to +6 at 95°C in 10⁻²M solutions.

- First demonstration and analysis of the combined effects of alloy species on the combined activation energy of film-free dissolution. (with M. Rockel)
- First demonstration, as in Figure 12, that the strain-induced dissolution transient can predict the occurrence of stress corrosion cracking. (with T. Shibata)

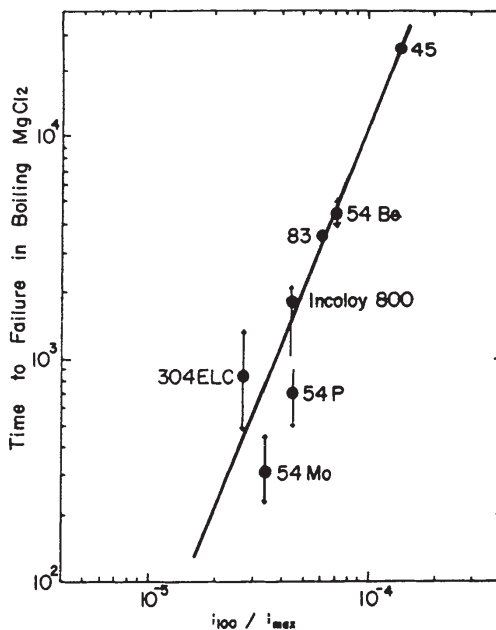


Figure 12 Time-to-failure in boiling MgCl₂ versus the ratio of current at 100 seconds to the maximum current for commercial and laboratory heats of Fe-Cr-Ni alloys.